NASA/CR-2000-210543
ICASE Report No. 2000-37

Discontinuous Dual-primal Mixed Finite Elements for Elliptic Problems

Carlo L. Bottasso, Stefano Micheletti, and Riccardo Sacco
Politecnico di Milano, Milano, Italy

ICASE
NASA Langley Research Center
Hampton, Virginia

Operated by Universities Space Research Association

National Aeronautics and
Space Administration

Langley Research Center
Hampton, Virginia 23681-2199

Prepared for Langley Research Center
under Contract NAS1-97046

October 2000

DISCONTINUOUS DUAL-PRIMAL MIXED FINITE ELEMENTS FOR ELLIPTIC PROBLEMS

CARLO L. BOTTASSO*, STEFANO MICHELETTI†, AND RICCARDO SACCO‡

Abstract. We propose a novel discontinuous mixed finite element formulation for the solution of second-order elliptic problems. Fully discontinuous piecewise polynomial finite element spaces are used for the trial and test functions. The discontinuous nature of the test functions at the element interfaces allows to introduce new boundary unknowns that, on the one hand enforce the weak continuity of the trial functions, and on the other avoid the need to define a priori algorithmic fluxes as in standard discontinuous Galerkin methods. Static condensation is performed at the element level, leading to a solution procedure based on the sole interface unknowns.

The resulting family of discontinuous dual-primal mixed finite element methods is presented in the one and two-dimensional cases. In the one-dimensional case, we show the equivalence of the method with implicit Runge-Kutta schemes of the collocation type exhibiting optimal behavior. Numerical experiments in one and two dimensions demonstrate the order accuracy of the new method, confirming the results of the analysis.

Subject classification. Applied and Numerical Mathematics

Key words. finite element method, mixed methods, discontinuous Galerkin, Petrov-Galerkin, elliptic problem

1. Introduction and Motivation. We consider the following classical model problem:

$$\begin{cases} -\mathrm{div}(\nu \underline{\nabla} u) = f & \text{in } \Omega \subset \mathbb{R}^2, \\ u = g & \text{on } \partial\Omega, \end{cases} \tag{1.1}$$

where Ω is a bounded polygon with Lipschitz boundary $\Gamma = \partial\Omega$, and ν, f, g are given functions. Dirichlet boundary conditions are considered only for the sake of simplicity, but the extension to the case of more general boundary data is straightforward. Definitions of functional and geometrical entities are given in section 2.

In view of the approximation of (1.1), we let $\{\mathcal{T}_h\}_{h>0}$ be a family of triangulations of $\overline{\Omega}$ and, for any $\mathcal{T}_h$, we denote by T any element thereof. Introducing the auxiliary unknown $\underline{\sigma} = \nu \underline{\nabla} u$, problem

*Dipartimento di Ingegneria Aerospaziale, Politecnico di Milano, Via La Masa 34, 20158 Milano, Italy (email: Carlo.Bottasso@polimi.it). This research was supported by the National Aeronautics and Space Administration under NASA Contract No. NAS1-97046 while the first author was in residence at ICASE, NASA Langley Research Center, Hampton, VA 23681-2199.

†Dipartimento di Matematica "F. Brioschi", Politecnico di Milano, Via Bonardi 9, 20133 Milano, Italy (email: Stefano.Micheletti@polimi.it).

‡Dipartimento di Matematica "F. Brioschi", Politecnico di Milano, Via Bonardi 9, 20133 Milano, Italy (email: Riccardo.Sacco@polimi.it).

(1.1) can be reformulated in weak form over each element T of $\mathcal{T}_h$ as

$$\left\{ \begin{array}{l} \displaystyle\int_T \nu^{-1} \underline{\sigma} \cdot \underline{\tau} \, dx + \int_T u \, \mathrm{div} \underline{\tau} \, dx - \int_{\partial T} u \, \underline{\tau} \cdot \underline{n}_T \, ds = 0, \\ \displaystyle\int_T \underline{\sigma} \cdot \underline{\nabla} v \, dx - \int_{\partial T} v \, \underline{\sigma} \cdot \underline{n}_T \, ds = \int_T f v \, dx, \end{array} \right. \tag{1.2}$$

where $\underline{\tau}$ and v are smooth vector and scalar functions, respectively, on T, while $\underline{n}_T$ is the unit outward normal vector to ∂T.

A unified framework for the analysis of the Discontinuous Galerkin (DG) method applied to elliptic problems in the form (1.2) was provided in ref. [1]. We shall follow the same path in the following, since the proposed method fits well in that framework. The DG formulation at the discrete level reads (see also [9]): find $u_h \in U_h$ and $\underline{\sigma}_h \in \underline{\Sigma}_h$ such that $\forall T \in \mathcal{T}_h$

$$\left\{ \begin{array}{ll} \displaystyle\int_T \nu^{-1} \underline{\sigma}_h \cdot \underline{\tau}_h \, dx + \int_T u_h \, \mathrm{div} \underline{\tau}_h \, dx - \sum_{\underline{e} \in \partial T} \int_{\underline{e}} h_u \underline{\tau}_h \cdot \underline{n}_T \, ds = 0 & \forall \underline{\tau}_h \in \underline{\Sigma}(T), \\ \displaystyle\int_T \underline{\sigma}_h \cdot \underline{\nabla} v_h \, dx - \sum_{\underline{e} \in \partial T} \int_{\underline{e}} v_h \underline{h}_\sigma \cdot \underline{n}_T \, ds = \int_T f v_h \, dx & \forall v_h \in U(T), \end{array} \right. \tag{1.3}$$

where $\underline{\Sigma}(T)$ and $U(T)$ are two sets of smooth vector and scalar functions, typically polynomials, defined on each element T, while $\underline{\Sigma}_h$ and U_h are the corresponding global finite element spaces. We are now dealing with a Galerkin method where the values of the unknown fields on each edge $\underline{e}$ of ∂T, noted $u_h|_{\underline{e}}$ and $\underline{\sigma}_h|_{\underline{e}}$, have been replaced by the *numerical fluxes* h_u and $\underline{h}_\sigma$. In practical implementations, h_u and $\underline{h}_\sigma$ are chosen as functions of the internal unknowns u_h and $\underline{\sigma}_h$ on two neighboring triangles. In particular, it can be shown that most methods reported in the literature can be classified based on the particular choice of the numerical fluxes h_u and $\underline{h}_\sigma$, choice often inspired by ideas borrowed from finite volume methods. The interested reader can consult ref. [1] for exact details on the expressions of the fluxes in the different cases.

It is clear that any particular choice on the nature of the numerical fluxes will affect the resulting scheme, eventually determining its numerical characteristics, stability, accuracy as well as the pattern of the stiffness matrix. This approach to the choice of the numerical fluxes is somewhat unsatisfactory, in the sense that it seems to be a rather artificial and dogmatic process, in some sense a "violence" to the underlying weak form (1.2). In this work, we shall therefore depart from the classical approach of defining *a priori* the expressions of the numerical fluxes. Hence, the interface fields h_u and $\underline{h}_\sigma \cdot \underline{n}_T$ are assumed to represent *new additional problem unknowns*, and we let the method implicitly define their values. In doing so, we obtain a genuine Petrov-Galerkin version of the DG method.

This formulation generalizes the method described in refs. [2, 3, 4, 5] to multiple spatial dimensions. In the one-dimensional case, the method can be shown to be equivalent to collocation-type implicit Runge-Kutta (RK) schemes. In particular, when used in conjunction with Gauss-Legendre quadrature, the finite element method here proposed corresponds to the Kuntzmann-Butcher (Gauss) RK scheme, which enjoys well known properties of *optimality*. This provides a strong motivation for seeking an extension of those ideas to the multi-dimensional case, extension that is attempted in this work for the elliptic boundary-value problem.

The paper is laid out as follows. Section 2 presents the proposed method for the classical problem of the Laplacian. Section 3 deals with the one-dimensional formulation of the present method and

with its connections with the time finite element and RK methods of refs. [2, 3, 4, 5]. In doing so, we shall temporarily abandon the simple linear model problem, and present the method for a general non-linear ODE problem. Section 4 is devoted to the description of the method in the two-dimensional case. Numerical results are discussed in section 5, where the proposed method is validated on one and two-dimensional test cases. Finally, the conclusions are discussed in section 6.

2. The Discontinuous Dual-Primal Mixed Method for a Model Problem. We are now ready to define the proposed Discontinuous Dual-Primal Mixed (DDPM) discretization of the one-element weak formulation of problem (1.1): find $u_h \in U_h$, $\underline{\sigma}_h \in \underline{\Sigma}_h$, $\lambda_h \in \Lambda_{h,g}$ and $\mu_h \in \Lambda_h$ such that $\forall T \in \mathcal{T}_h$ we have

$$\begin{cases} \displaystyle\int_T \nu^{-1}\underline{\sigma}_h \cdot \underline{\tau}_h \, dx + \int_T u_h \, \mathrm{div}\underline{\tau}_h \, dx - \int_{\partial T} \lambda_h \underline{\tau}_h \cdot \underline{n}_T \, ds = 0 & \forall \underline{\tau}_h \in \underline{W}(T), \\ \displaystyle\int_T \underline{\sigma}_h \cdot \underline{\nabla} v_h \, dx - \int_{\partial T} \mathcal{S}_T v_h \mu_h \, ds = \int_T f v_h \, dx & \forall v_h \in V(T). \end{cases} \tag{2.1}$$

The meaning of the symbols is as follows. For any $\mathcal{T}_h \in \{\mathcal{T}_h\}_{h>0}$, let $\mathcal{E}_h$ be the associated set of edges. For any edge $\underline{e}$ of $\mathcal{E}_h$, we denote by $\underline{n}_e$ the unit normal vector to $\underline{e}$, directed according to a uniquely fixed arbitrary convention. Namely, $\underline{n}_e$ coincides with the unit outward normal vector on the boundary Γ if $\underline{e} \cap \Gamma \neq \emptyset$, otherwise $\underline{n}_e$ coincides with one of the two outward normals to the triangles sharing the edge $\underline{e}$ if $\underline{e} \cap \Gamma = \emptyset$. Then, for any $T \in \mathcal{T}_h$ we denote by $\underline{n}_T$ the unit outward normal vector to ∂T and define the sign function $\mathcal{S}_T = \underline{n}_e \cdot \underline{n}_T = \pm 1$. Through the use of $\mathcal{S}_T$, we can associate the interface degrees of freedom with mesh edges, so that the sign function will determine whether a given flux μ_h is entering of exiting from a given triangle. For simplicity, we shall omit in the following the dependence of $\underline{n}$ on the edge $\underline{e}$ which will be understood.

Given the fact that the edge fluxes are now unknowns to the problem, we can not choose test and trial functions within the same spaces, as for the DG method (1.3). Therefore, we are now dealing with a Petrov-Galerkin formulation. The global finite element spaces for the internal variables $\underline{\sigma}_h$ and u_h are defined as

$$\begin{aligned} \underline{\Sigma}_h &= \left\{ \underline{v}_h \in \underline{L}^2(\Omega) \,|\, \underline{v}_h|_T \in \underline{\Sigma}(T) \, \forall T \in \mathcal{T}_h \right\}, \\ U_h &= \left\{ v_h \in L^2(\Omega) \,|\, v_h|_T \in U(T) \, \forall T \in \mathcal{T}_h \right\}, \end{aligned}$$

where $\underline{L}^2(\Omega) = (L_2(\Omega))^2$. Considering now the interface fields λ_h and μ_h, we note that they represent the traces of u and $\underline{\sigma} \cdot \underline{n}_T$ on ∂T, respectively. Using the language of computational mechanics, the new unknowns act as "mixed connectors" between neighboring triangles (see [16] and [18], Chapter 13). We let $\Lambda(\underline{e})$ indicate a set of scalar smooth functions defined on each edge $\underline{e}$. Then, we define the (global) finite dimensional spaces

$$\begin{aligned} \Lambda_h &= \left\{ \eta_h \in L^2(\mathcal{E}_h) \,|\, \eta_h|_{\underline{e}} \in \Lambda(\underline{e}) \, \forall \underline{e} \in \mathcal{E}_h \right\}, \\ \Lambda_{h,g} &= \left\{ \eta_h \in \Lambda_h \,|\, \eta_h = \mathcal{P} g \, \text{if} \, \underline{e} \cap \Gamma \neq \emptyset \right\}, \end{aligned}$$

where $\mathcal{P}$ is the L^2-projection operator on $\Lambda(\underline{e})$. Finally, we introduce the local and global finite element spaces for the test functions $\underline{\tau}$ and v. Denoting by $\underline{W}(T)$ and $V(T)$ two sets of smooth vector and

scalar functions defined on each element T, we have

$$\underline{W}_h = \left\{ \underline{\tau}_h \in \underline{L}^2(\Omega) \,|\, \underline{\tau}_h|_T \in \underline{W}(T) \,\forall T \in \mathcal{T}_h \right\},$$
$$V_h = \left\{ w_h \in L^2(\Omega) \,|\, w_h|_T \in V(T) \,\forall T \in \mathcal{T}_h \right\}.$$

The choice of the functional spaces will be detailed in the following sections for the one and the two-dimensional case.

We note that the method is *completely conservative* in the sense of ref. [1], since the interface unknowns are associated with edges and are consequently identical for two triangles sharing the edge. This last property implies the following conservation statement

$$\sum_{\underline{e} \in \partial U} \int_{\underline{e}} \mu_h \, ds + \int_U f \, dx = 0,$$

where U is the union of some collection of elements, and v_h was taken to be identically unity in the second of (2.1).

The DDPM approach can be viewed as a consistent hybridization of the dual-primal mixed (DPM) method introduced in ref. [12]. Indeed, the spirit of the standard hybridization procedure (see [7], Chapter V) is to relax the continuity of some of the unknowns ($\underline{\sigma} \cdot \underline{n}$ in the dual hybrid philosophy or u in the primal hybrid philosophy) and then to enforce it back through the introduction of suitable inter-element Lagrange multipliers. Precisely, $u|_{\underline{e}}$ represents the Lagrange multiplier in the case of dual hybrid methods, while $\underline{\sigma} \cdot \underline{n}|_{\underline{e}}$ is the Lagrange multiplier in the case of primal hybrid methods. In the present case, we relax the continuity of *both* u and $\underline{\sigma} \cdot \underline{n}$ in the interior fields and let the interface variables connect neighboring elements. The interface variables λ and μ do not play the role of Lagrange multipliers in our case but, nevertheless, enjoy appealing properties. Physically, they have the clear meaning of $u|_{\underline{e}}$ and $\underline{\sigma} \cdot \underline{n}|_{\underline{e}}$, respectively, while numerically they exhibit a higher rate of convergence than the internal variables, as it will be shown in the following. This is also a feature of the Lagrange multipliers in the case of standard hybrid methods ([7], Chapter V).

Alternatively, one could note that, by gluing the test functions together at neighboring triangles, each internal edge receives equal and opposite contributions from the two elements using it, and therefore the boundary unknowns are eliminated. This way one recovers from (2.1) the DPM method.

3. The DDPM Method in the One-Dimensional Case. We abandon now for the moment the linear model problem (1.1), and we consider a generic system of first order ODE's

$$\underline{z}' = \underline{f}(\underline{z}, x), \tag{3.1}$$

where $\underline{z}, \underline{f} \in \mathbb{R}^D$ and D is the number of state variables. Suitable initial or two-point boundary conditions complement problem (3.1). In the case of the linear model problem, we clearly have $\underline{z} = (u, \sigma)^T$ and $\underline{f} = (\sigma, -f)^T$. However, since the discussion can be easily completed for the more general case, we consider (3.1) instead of the one-dimensional version of (1.1) in the remainder of this section.

We assume $\Omega = (0, X)$ and let $0 \equiv x_0 < x_1 < \ldots < x_{n-1} < x_n \equiv X$ be a given partition $\mathcal{T}_h$ of $\overline{\Omega}$ into $n \geq 1$ intervals $T_i = [x_i, x_{i+1}]$ of size h_i, $i = 0, \ldots, n-1$, where $\{x_i\}_{i=0}^n$ are the nodes. Note that in the one-dimensional case $\mathcal{E}_h \equiv \{x_i\}_{i=0}^n$ and each edge $\underline{e}$ degenerates into one single node.

The statement of the present finite element method is as follows: find $(\underline{z}_h, \underline{\lambda}_h) \in (\underline{Z}_h \times \underline{\Lambda}_h)$ such that for each $T_i \in \mathcal{T}_h$, $i = 0, \ldots, n-1$, the following holds

$$\int_{T_i} \underline{z}_h \cdot \underline{w}_h' \, dx + \int_{T_i} \underline{f}(\underline{z}_h, x) \cdot \underline{w}_h \, dx - (\underline{\lambda}_{i+1} \cdot \underline{w}_h(x_{i+1}) - \underline{\lambda}_i \cdot \underline{w}_h(x_i)) = 0$$
$$\forall \underline{w}_h \in \underline{W}(T_i). \quad (3.2)$$

For any $T \in \mathcal{T}_h$, we define the local finite element spaces for the internal fields $\underline{z}_h$ and for the test functions as follows:

$$\underline{Z}(T) = (\mathbb{P}_k(T))^D, \qquad \underline{W}(T) = (\mathbb{P}_{k+1}(T))^D,$$

with $k \geq 0$. The local finite element space for the interface unknowns $\underline{\lambda}_h$ is

$$\underline{\Lambda}(\partial T_i) = \{\underline{\lambda}_i, \underline{\lambda}_{i+1}\}, \qquad i = 0, \ldots, n-1,$$

where for any function $\underline{\lambda} \in \underline{\Lambda}(\partial T_i)$ we let $\underline{\lambda}_i = \underline{\lambda}(x_i)$ and $\underline{\lambda}_{i+1} = \underline{\lambda}(x_{i+1})$, $i = 0, \ldots, n-1$. Furthermore, we set

$$\underline{\mathcal{U}}(T) = \underline{U}(T) \times \underline{\Lambda}(\partial T), \qquad \underline{\mathcal{V}}(T) = \underline{W}(T).$$

The finite element space is then

$$\mathbb{DP}_k(T) = \{(\underline{z}, \underline{\lambda}; \underline{w}) \,|\, (\underline{z}, \underline{\lambda}; \underline{w}) \in \underline{\mathcal{U}}(T) \times \underline{\mathcal{V}}(T) \, \forall T \in \mathcal{T}_h\}. \quad (3.3)$$

The global finite element spaces for the internal fields and the test functions are

$$\underline{Z}_h = \left\{\underline{z}_h \in (L^2(\Omega))^D \,|\, z_h|_T \in \underline{Z}(T) \, \forall T \in \mathcal{T}_h\right\},$$
$$\underline{W}_h = \left\{\underline{w}_h \in (L^2(\Omega))^D \,|\, w_h|_T \in \underline{W}(T) \, \forall T \in \mathcal{T}_h\right\},$$

while the global spaces for the interface unknowns are

$$\underline{\Lambda}_h = \left\{\{\underline{\lambda}_i\}_{i=0}^n \,|\, \underline{\lambda}_i \in \mathbb{R}^D, \, i = 0, \ldots, n\right\},$$

where functions are defined only at the nodes of $\mathcal{E}_h$. Finally, gathering the previous definitions, we obtain the global finite element space as

$$\mathbb{DP}_h^k = (\underline{Z}_h \times \underline{\Lambda}_h) \times \underline{W}_h. \quad (3.4)$$

It is clear that both initial and boundary-value problems can be solved within this framework. For an initial value problem, one can solve marching sequentially in an element-by-element fashion, as with any time stepping procedure. We have: $\dim(\underline{Z}(T)) = D(k+1)$, $\dim(\underline{W}(T)) = D(k+2) \, \forall T \in \mathcal{T}_h$. Therefore, for any $T \in \mathcal{T}_h$, (3.2) leads to a system of $D(k+2)$ equations in the $D(k+1) + 2D$ local unknowns $\underline{z}_h|_T$, $\underline{\lambda}_h|_T$, leaving space for the D initial conditions that complement problem (3.1). A boundary-value problem leads to a global discrete problem defined over Ω. In this case we have $nD(k+2)$ equations in the $nD(k+1)+2nD$ unknowns. However, considering that $\underline{\lambda}_{i+1}$ appears in both neighboring elements T_i and T_{i+1}, the total unknown count is reduced to $nD(k+1)+2nD-(n-1)D$,

which leaves once again space for D two-point boundary values. In both cases, the internal field $\underline{z}_h$ can be eliminated at the element level in favor of the interface unknowns $\underline{\lambda}_h$, and then recovered at convergence.

We note that the scheme presents two jump discontinuities for each finite element, namely one at x_i and the other at x_{i+1}, since $\underline{\lambda}_i \neq \underline{z}_h(x_i)$ and $\underline{\lambda}_{i+1} \neq \underline{z}_h(x_{i+1})$. For this reason it was termed the Bi-Discontinuous (BD) scheme in ref. [3]. It is clear that such symmetric treatment of the element boundaries implies no privilege in the direction of the flow of information, and it is therefore best suited for two-point boundary-value problems.

Quite differently, for initial value problems it is sometimes desirable to have stiffly accurate schemes, that are able to damp the higher frequencies components from the computed response [11]. This is achieved in practice by forcing a lack of symmetry in the scheme, that incorporates the knowledge on the direction of flow of information within the element. It is possible to derive such schemes in the present framework, allowing one single jump discontinuity at x_i while enforcing the condition $\underline{\lambda}_{i+1} = \underline{z}_h(x_{i+1})$. One obtains in this case the so called Singly-Discontinuous (SD) schemes [3].

3.1. Equivalence with Runge-Kutta Methods. It was shown in ref. [3] and then again with a slightly different proof in ref. [4], that the finite element method (3.2) can be written as a RK process for any order k. RK methods are probably best known for the solution of initial value problems, but clearly can also be used for the solution of two-point boundary-value problems by assembling the single steps to yield a global discrete problem defined over the whole computational domain, exactly as in the finite element method. Since the link between the two approaches seems to be useful in the characterization of the proposed method, we briefly review this result in the following.

We begin by selecting a quadrature rule for the evaluation of the integrals in (3.2). The rule is defined by s abscissæ c_i and weights b_i. We consider the case $s = k + 1$, therefore the number of quadrature points is the same as the number of finite element nodes of the trial functions.

Following the usual FEM practice, one expresses the discrete equations in terms of the nodal values. Here we shall take a different approach, and *assume as unknowns the values of the finite element trial functions at the quadrature points.* This is the key idea for showing the link existing between finite element and RK methods. The change of unknowns can be done because we are using a quadrature rule that uses as many integration points as the number of finite element nodes, as previously said. We will come back later to some interesting consequences of this assumption.

We first note that the test functions can be expressed as

$$\underline{w}_h = \sum_{i=1}^{k+2} \tau^{i-1} \underline{\alpha}_i, \tag{3.5}$$

where τ^j are polynomials, $\tau \in \mathbb{R}$, and $\underline{\alpha}_k$ their associated amplitudes. Next, let us define the $(s+1) \times s$ matrix $P_\xi = \left[\tau^{i-1}|_{\tau=\xi_j}\right]$, with $i = 1, \ldots, s+1$, $j = 1, \ldots, s$, the ξ_j's being s real values. The derivative of P_ξ with respect to τ is then $P'_\xi = \left[(i-1)\tau^{i-2}|_{\tau=\xi_j}\right]$. Note that, for any choice of the ξ_j's, the first row of P_ξ is all made of one's, and the first row of P'_ξ is all made of zero's. For $\xi_j = c_j$, we have the matrices $P_c = \left[c_j^{i-1}\right]$, $P'_c = \left[(i-1)c_j^{i-2}\right]$. We also define the $s \times s$ diagonal matrix $B = \left[\begin{smallmatrix} \ddots & \\ & b_i \end{smallmatrix}\right]$, with $i = 1, \ldots, s$, and the following s-dimensional vectors: $\underline{b} = (b_1, b_2, \ldots, b_s)^T$, $\underline{c} = (c_1, c_2, \ldots, c_s)^T$, and

$\underline{0} = (0, 0, \ldots, 0)^T$, $\underline{1} = (1, 1, \ldots, 1)^T$, $\underline{1}_1 = (1, 0, \ldots, 0)^T$.

We note that

$$P_c' B = \begin{bmatrix} \underline{0}^T \\ Q' \end{bmatrix}, \tag{3.6}$$

Q being the $s \times s$ matrix $Q = \left[\tau^i|_{\tau=c_j} b_j\right] = \left[c_j^i b_j\right]$. The derivative of Q with respect to τ is given by $Q' = \left[i\, c_j^{i-1} b_j\right]$. Furthermore, if the quadrature formula is of order s, we have that

$$Q' \underline{1} = \underline{1}. \tag{3.7}$$

Equation (3.7) corresponds to the so called *"B simplifying assumption"* in the theory of RK methods.

The discrete weak form (3.2) can now be written as

$$((P_c' B) \otimes \mathbb{I}_D)\, \hat{\underline{z}} + h_i((P_c B) \otimes \mathbb{I}_D)\, \hat{\underline{f}} = (\underline{1} \otimes \mathbb{I}_D)\, \underline{\lambda}_{i+1} - (\underline{1}_1 \otimes \mathbb{I}_D)\, \underline{\lambda}_i, \tag{3.8}$$

where the following two sD-dimensional vectors were defined: $\hat{\underline{z}} = (\underline{z}^1, \ldots, \underline{z}^s)^T$, $\hat{\underline{f}} = (\underline{f}(\underline{z}^1, x_i + c_1 h_i), \ldots, \underline{f}(\underline{z}^s, x_i + c_s h_i))^T$. $\mathbb{I}_D$ is the $D \times D$ identity matrix, while $\otimes$ denotes the tensor Kronecker product of matrices, so that $(\cdot) \otimes \mathbb{I}_D$ ensures that all degrees of freedom of the vectorial problem are integrated according to the same rule.

Solving for $\hat{\underline{z}}$ and $\underline{\lambda}_{i+1}$ and using (3.7), we have

$$(\hat{\underline{z}}, \underline{\lambda}_{i+1})^T = \begin{bmatrix} \underline{1} & h_i(\underline{1}\underline{b}^T - Q'^{-1} Q) \\ 1 & h_i \underline{b}^T \end{bmatrix} \otimes \mathbb{I}_D (\underline{\lambda}_i, \hat{\underline{f}})^T. \tag{3.9}$$

From this expression, we conclude that (3.2) can be written as a s-stage RK method whose tableau [10] is given by

$$\begin{array}{c|c} \underline{c} & \underline{1}\underline{b}^T - Q'^{-1} Q \\ \hline & \underline{b}^T \end{array}. \tag{3.10}$$

Finally, we test the Gauss-Legendre, Lobatto and Radau quadrature rules and compute the corresponding tableaux (3.10). The results are summarized in Table (3.1).

TABLE 3.1
Correspondence between quadrature rules for BD finite elements and RK methods.

Quadrature Rule	RK Method
Gauss	Kuntzmann-Butcher
Lobatto	Lobatto IIIB
Radau-Left	Radau IA

Table (3.1) shows that the family of schemes deriving from the one-dimensional finite element method considered in this work corresponds to some well known RK algorithms. The two approaches differ on the choice of the unknowns: the finite element method solves for the *nodal values*, while

the RK method solves for the *quadrature point values*. However, these two sets of values are simply related by a linear transformation. Furthermore, note that all RK schemes appearing in the table are of the collocation type, where polynomials interpolate the two interface values $\underline{\lambda}_i$, $\underline{\lambda}_{i+1}$ and the internal stages $\hat{\underline{z}}$ [10]. This link between finite elements and RK processes allows a somewhat unique way of looking at the discretization procedure: from the finite element point of view we see jumps in the field variables, since we have discontinuous interpolations of the internal fields, glued together from one element to its neighbor through the presence of the interface unknowns. Quite differently, from the RK point of view we have continuous interpolations of the interface unknowns with internal variables at the collocation points, with apparently no jump discontinuities in the solution. It should also be remarked that for these RK methods, maximal order is in general attained only at the interface values, and not at the internal stages. We then expect to observe higher rates of convergence of the interface fields also in the multi-dimensional generalization of the method.

The same table shows that the present finite element formulation, when used in conjunction with Gauss-Legendre quadrature, yields the Kuntzmann-Butcher (or Gauss) RK methods. These RK schemes are probably the ones that enjoy the greatest number of numerical properties, and are in this sense optimal. In fact they are of maximal order $(2s)$, they are algebraically stable, and also symplectic when applied to Hamiltonian systems [17]. Simplecticity is the distinguishing property of Hamiltonian systems, and its numerical preservation has a strong influence on the behavior of the integration scheme.

As a final point, we note that these results are solely based on having assumed a quadrature rule that uses as many points as the number of finite element nodes. In reality, working from the point of view of the finite element method, one could choose to use a *greater* number of quadrature points, for example in the hope of improving the accuracy in the evaluation of strongly non-linear functions in the term $\int_{T_i} \underline{f}(\underline{z}_h, x) \cdot \underline{w}_h \, dx$. It can be shown however, that increasing the number of quadrature points can in reality *degrade* the performance of the method. For example, using a larger number of points destroys the symplectic nature of the scheme [3].

4. The Two-Dimensional Case. For two spatial dimensions, the choice of the finite element spaces for the internal and interface unknowns is a straightforward extension of those introduced in the one-dimensional case. Precisely, for $k \geq 0$ we set

$$\underline{\Sigma}(T) = \left(\mathbb{P}_k(T)\right)^2, \quad U(T) = \mathbb{P}_k(T) \qquad \forall T \in \mathcal{T}_h,$$
$$\Lambda(\underline{e}) = \mathbb{P}_k(\underline{e}) \qquad \forall \underline{e} \in \mathcal{E}_h.$$

The choice of the finite element test spaces is less obvious and requires some care. Here we focus on the description of the method in the cases $k = 0$ and $k = 1$. We start by introducing the Raviart-Thomas finite element space of degree k [14]

$$\mathbb{RT}_k(T) = \left(\mathbb{P}_k(T)\right)^2 \oplus \underline{x}\mathbb{P}_k(T) \qquad \forall T \in \mathcal{T}_h.$$

In the case of the $\mathbb{DP}_h^0$ finite elements, we set $\underline{W}(T) = \mathbb{RT}_0(T)$ and $V(T) = \mathbb{P}_1(T)$. The global finite element spaces $\underline{W}_h$ and V_h are then simply defined as the products of the corresponding local spaces.

Notice that $\underline{W}_h$ and V_h are the *discontinuous* counterparts of the corresponding test spaces that have been used in the dual-primal formulation of ref. [12].

In the case of the $\mathbb{DP}_h^1$ finite elements, we set $\underline{W}(T) = \mathbb{RT}_1(T)$ and $V(T) = \mathbb{P}_2(T) \oplus \mathcal{B}_3(T)$ for each $T \in \mathcal{T}_h$. $\mathcal{B}_3(T)$ is the following cubic bubble [15]

$$\mathcal{B}_3 = (\varphi_0 - \varphi_1)(\varphi_1 - \varphi_2)(\varphi_2 - \varphi_0),$$

where $\varphi_i = \varphi_i(\underline{x})$, $i = 0, 1, 2$, are the centroidal coordinates of a point $\underline{x} \in \mathbb{R}^2$ with respect to the vertices of T. Enrichment of the scalar test space is a standard procedure in hybrid methods when the degree of the polynomials in $V(T)$ is even (see refs. [15, 8]). Actually, one can check that without adding the cubic bubble the rectangular matrix arising from the integral $\int_{\partial T} \mathcal{S}_T v_h \mu_h \, ds$ becomes rank deficient.

As far as the implementation is concerned, we point out that for both the $k = 0$ and $k = 1$ cases it is possible to perform a static condensation of the internal variables in favor of the edge unknowns, obtaining a linear system in the sole interface variables λ_h and μ_h.

The generalization of the DDPM method to higher orders will be more extensively addressed in a forthcoming paper. Let us just mention that a possible general recipe for constructing the $\mathbb{DP}_h^k$ finite element spaces for even k can be given as

$$\underline{W}(T) = BDFM_{k+1}(T), \qquad V(T) = \mathbb{P}_{k+1}(T) \qquad \forall T \in \mathcal{T}_h,$$

where $BDFM_{k+1}$ is the triangular analogue of the reduced element introduced in ref. [6].

5. Numerical Results. In this section we demonstrate the $\mathbb{DP}_h^k$ finite elements for $k = 0$ and $k = 1$ through the solution of test cases in both one and two spatial dimensions.

5.1. One-Dimensional Examples. We consider the following two-point boundary-value model problem

$$\begin{cases} -(\nu(x)u'(x))' = f(x), & 0 < x < 1, \\ u(0) = u(1) = 0. \end{cases} \tag{5.1}$$

In all numerical experiments, successively finer uniform grids of size $h = 2^{-j}$, $j \in \{1, \ldots, 9\}$ are used. We set $e_u = u - u_h$ and $e_\sigma = \sigma - \sigma_h$; moreover e_λ and e_μ denote the functions defined only at the nodes of $\mathcal{E}_h$ such that $e_\lambda(x_i) = u(x_i) - \lambda_i$ and $e_\mu(x_i) = \sigma(x_i) - \mu_i$, $i = 0, \ldots, n$.

For any function $v \in L^2(\Omega)$ and sufficiently smooth on each $T \in \mathcal{T}_h$, we denote by $I_{1,T}(v)$ the approximation of $\int_T v \, dx$ using the trapezoidal rule. Moreover, for each $T \in \mathcal{T}_h$ we denote by $\{\overline{x}_{j,T}^k\}_{j=0}^k$ the $k+1$ Gauss-Legendre points on T. In order to measure the convergence rate of the $\mathbb{DP}_h^k$ finite elements, we use the following three norms:

$$\|v\|_{h,0,\Omega} = \left(\sum_{i=0}^{n-1} I_{1,T_i}(v^2) \right)^{1/2},$$

$$\|w\|_{h,GP,\infty} = \begin{cases} \max\limits_{i \in \{0,\cdots,n-1\}} |w(\overline{x}_{0,T}^0))|, & \text{if } k = 0, \\ \max\limits_{i \in \{0,\cdots,n-1\}} \left(\max\limits_{j \in \{0,1\}} (|w(\overline{x}_{j,T}^1)|) \right), & \text{if } k = 1, \end{cases}$$

$$\|\eta\|_{h,\infty} = \max_{i \in \{0,\cdots,n\}} |\eta_i|,$$

where w is any bounded function defined at the Gauss points of $\mathcal{T}_h$ and η is any bounded function defined at the nodes of $\mathcal{T}_h$. Clearly, $\|\cdot\|_{h,0,\Omega}$ is a discrete $L^2(\Omega)$ norm, while the other two norms are discrete maximum norms over the set of Gauss points and $\mathcal{E}_h$, respectively. The quadrature formula used in the discrete norm is accurate enough not to pollute the computed accuracy, and at the same time avoids to sample the solution at superconvergent points. Moreover, observe that any integral appearing in the DDPM discretization of (5.1) has been computed using a one-point Gauss-Legendre quadrature rule (with node x_0^0 on each $T \in \mathcal{T}_h$) for $k = 0$ and a two-point Gauss-Legendre quadrature rule (with nodes $\{\overline{x}_{j,T}^1\}_{j=0}^1$ on each $T \in \mathcal{T}_h$) for $k = 1$.

The following symbols are used in the graphs: for any h, symbol '*' refers to $\|e_u\|_{h,0,\Omega}$ (or $\|e_\sigma\|_{h,0,\Omega}$), while symbols '□' and 'o' denote $\|e_u\|_{h,GP,\infty}$ (or $\|e_\sigma\|_{h,GP,\infty}$) and $\|e_\lambda\|_{h,\infty}$ (or $\|e_\mu\|_{h,\infty}$), respectively.

Test Case 1 We set $\nu(x) = 1$ and $f(x) = \sin(\pi x)$, $x \in [0,1]$. The exact solution is the smooth function $u(x) = (1/\pi^2)\sin(\pi x)$, which implies $\sigma(x) = u'(x) = (1/\pi)\cos(\pi x)$. We show in figure 5.1 the error curves for e_u and e_λ (left) and e_σ and e_μ (right) in the case $k = 0$. The corresponding error curves in the case $k = 1$ are shown in figure 5.2.

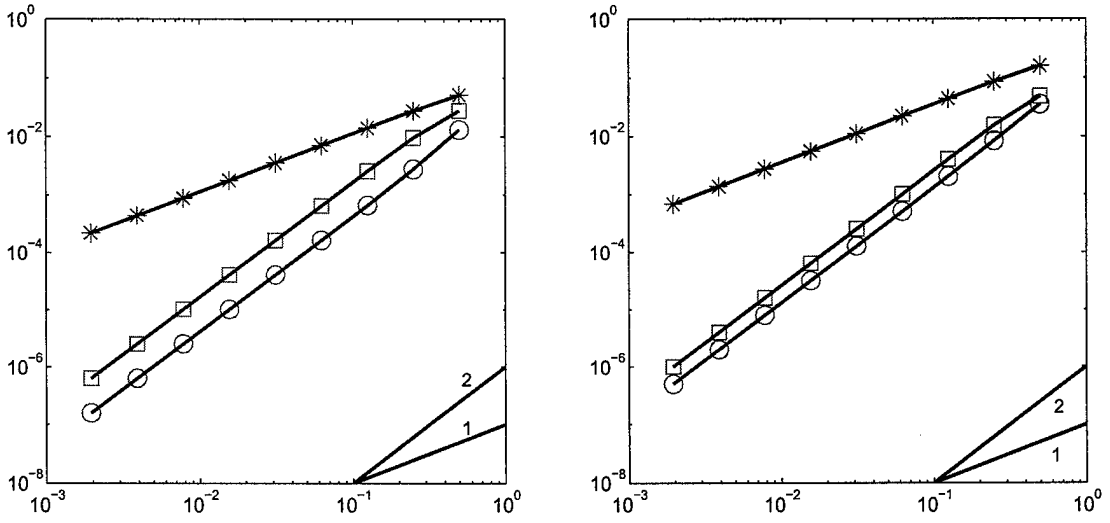

FIG. 5.1. *One spatial dimensions, test case 1. Approximation errors e_u and e_λ (left) and e_σ and e_μ (right) for $\mathbb{DP}_h^0$ finite elements.*

The plots show second-order convergence for the interface unknowns in the case $k = 0$, while the internal unknowns are only first-order accurate. Superconvergence of the internal variables can be observed at the Gauss point. For the $\mathbb{DP}_h^1$ finite elements, the error curves show that the interface unknowns are fourth-order convergent, the internal fields are second-order accurate while a third-order convergence rate is exhibited by the internal unknowns at the two Gauss points of each element. All these results are in agreement with the theory of RK methods.

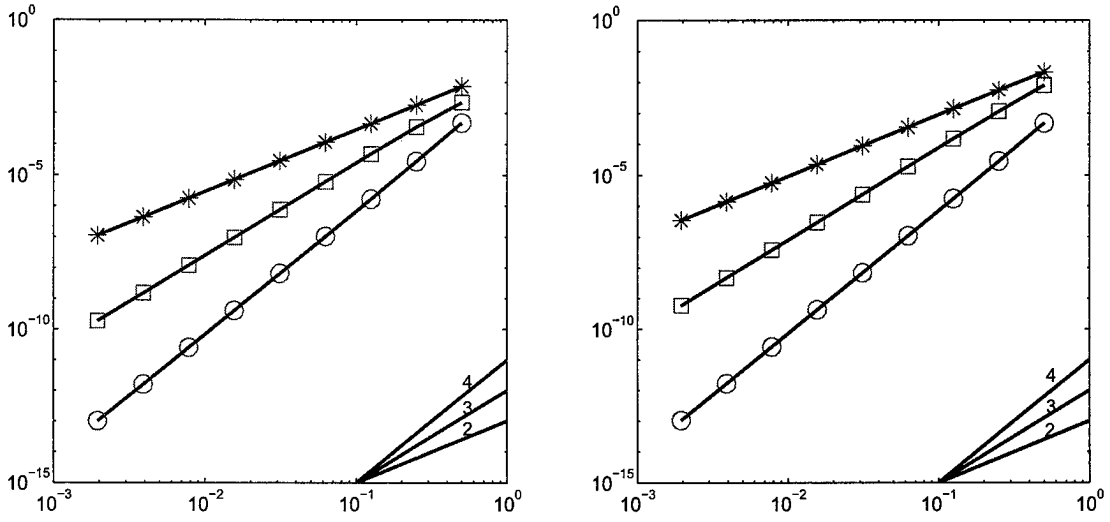

FIG. 5.2. *One spatial dimensions, test case 1. Approximation errors e_u and e_λ (left) and e_σ and e_μ (right) for $\mathbb{DP}^1_h$ finite elements.*

Test Case 2 This test problem demonstrates the performances of the DDPM method in the presence of strong solution gradients. The coefficient ν and the source term f are chosen as in ref. [13] (see also ref. [8], section 4.4.1, for further comments), and read

$$\nu(x) = \frac{1}{\alpha} + \alpha(x-\overline{x})^2,$$
$$f(x) = 2\left(1 + \alpha(x-\overline{x})\left\{\tan^{-1}(\alpha(x-\overline{x})) + \tan^{-1}(\alpha x)\right\}\right).$$

The exact solution is

$$u(x) = (1-x)\left(\tan^{-1}(\alpha(x-\overline{x})) + \tan^{-1}(\alpha x)\right),$$
$$\sigma(x) = \left(\frac{1}{\alpha} + \alpha(x-\overline{x})^2\right)\left\{-\tan^{-1}(\alpha(x-\overline{x})) - \tan^{-1}(\alpha x) + (1-x)\frac{\alpha}{1+\alpha^2(x-\overline{x})^2}\right\},$$

where $\sigma(x) = \nu(x)u'(x)$. Furthermore, we set $\alpha = 100$ and $\overline{x} = 0.36388$.

We show in figure 5.3 the error curves for e_u and e_λ (left) and e_σ and e_μ (right) in the case $k = 0$. The corresponding error curves in the case $k = 1$ are shown in figure 5.4.

The numerical results clearly show the increased "roughness" of the problem when compared with the corresponding error curves for test case 1. Nevertheless, all variables attain the expected convergence rate as $h \to 0$. Figure 5.5 shows the exact solution u (solid line) plotted against the finite element solution λ_h computed with $\mathbb{DP}^0_h$ elements and $h = 1/20$. Notice the sharp internal layer, resolved within one element.

5.2. Two-Dimensional Examples. For the two-dimensional case, we consider (1.1) in the square domain $\Omega = (-1,1)^2$ with $g = 0$. The exact solution is in this case $u(x,y) = (x^2-1)(y^2-1)$ and $\underline{\sigma}(x,y) = 2\left(x(y^2-1), y(x^2-1)\right)^T$; the right-hand side f is computed accordingly. In all numerical experiments, we use a uniform grid of isosceles right triangles of size $h_x = h_y = h$, where h takes on the values $2^{1-j}/5$, $j \in \{0,1,2,3\}$ for the $\mathbb{DP}^0_h$ case and $\{2/5, 2/10, 2/20, 2/30\}$ for the $\mathbb{DP}^1_h$ case.

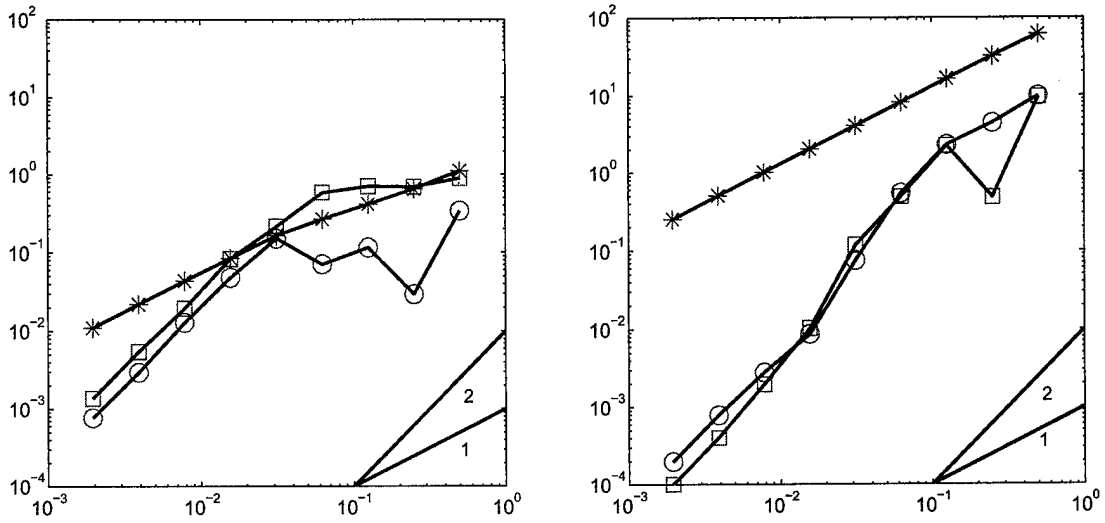

FIG. 5.3. *One spatial dimensions, test case 2. Approximation errors e_u and e_λ (left) and e_σ and e_μ (right) for $\mathbb{DP}_h^0$ finite elements.*

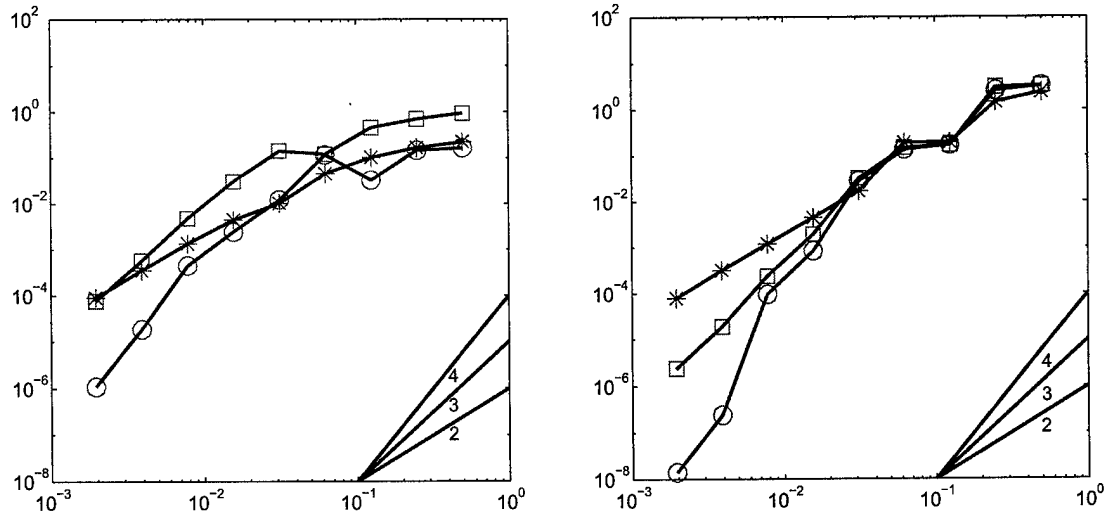

FIG. 5.4. *One spatial dimensions, test case 2. Approximation errors e_u and e_λ (left) and e_σ and e_μ (right) for $\mathbb{DP}_h^1$ finite elements.*

As in the one-dimensional examples, we denote by $e_u = u - u_h$ and $\underline{e}_\sigma = \underline{\sigma} - \underline{\sigma}_h$ the discretization errors associated with the internal fields, while $e_\lambda = \mathcal{P}\lambda - \lambda_h$ and $e_\mu = \mathcal{P}\mu - \mu_h$ are the discretization errors associated with the interface fields. $\mathcal{P}$ is the L^2-projection operator on $\Lambda(\underline{e})$, for each $\underline{e} \in \mathcal{E}_h$. Furthermore, for any $T \in \mathcal{T}_h$ we denote by $|T|$ the measure of T, by $\underline{a}_r$, $r = 0, 1, 2$ the vertices of T, by $\underline{x}_{C,T}$ the centroid of T and by $\underline{x}_{j,T}, j = 0, 1, 2$ the three Gauss points of T obtained from the area coordinates $\{2/3, 1/6, 1/6\}$ by permutation. In order to measure the convergence rate of the $\mathbb{DP}_h^k$

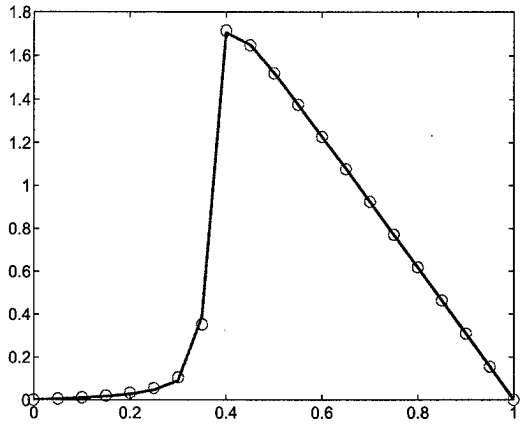

FIG. 5.5. *One spatial dimensions, test case 2. Exact solution (solid line) and numerical solution λ_h ('o') computed using $\mathbb{DP}_h^0$ finite elements ($h = 1/20$).*

finite elements, we introduce the following discrete norms:

$$\|v\|_{h,0,\Omega} = \left(\sum_{T \in \mathcal{T}_h} \frac{|T|}{3} \sum_{r=0}^{2} (v(\underline{a}_r))^2 \right)^{1/2},$$

$$\|v\|_{h,GP,\infty} = \begin{cases} \max\limits_{T \in \mathcal{T}_h} |v(\underline{x}_{C,T})|, & \text{if } k = 0, \\ \max\limits_{T \in \mathcal{T}_h} \max\limits_{j \in \{0,1,2\}} |v(\underline{x}_{j,T})|, & \text{if } k = 1, \end{cases}$$

$$\|\eta\|_{h,-1/2,\mathcal{E}_h} = \left(\sum_{\underline{e} \in \mathcal{E}_h} |\underline{e}| \|\eta\|_{0,\underline{e}}^2 \right)^{1/2},$$

where v is any sufficiently smooth function on T belonging to $L^2(\Omega)$, η is any function belonging to $L^2(\underline{e})$ for each $\underline{e} \in \mathcal{E}_h$ and $\|\eta\|_{0,\underline{e}}$ is the L^2-norm on edge $\underline{e}$. Notice that $\|\cdot\|_{h,0,\Omega}$ is a discrete $L^2(\Omega)$ norm, $\|\cdot\|_{h,GP,\infty}$ is a discrete $L^\infty(\Omega)$ norm, while $\|\cdot\|_{h,-1/2,\mathcal{E}_h}$ is a discrete $H^{-1/2}(\mathcal{E}_h)$ norm (see also ref. [7], Sect. V.3). For vector functions $\underline{v} = (v_1, v_2)^T$, the above norms are defined

$$\|\underline{v}\|_{h,0,\Omega} = \left(\textstyle\sum_{i=1,2} \|v_i\|_{h,0,\Omega}^2 \right)^{1/2},$$
$$\|\underline{v}\|_{h,GP,\infty} = \max_{i \in \{1,2\}} \|v_i\|_{h,GP,\infty}.$$

In the following figures, symbol '*' is used to denote $\|e_u\|_{h,0,\Omega}$ (or $\|\underline{e}_\sigma\|_{h,0,\Omega}$), while symbols '□' and 'o' denote $\|e_u\|_{h,GP,\infty}$ (or $\|\underline{e}_\sigma\|_{h,GP,\infty}$) and $\|e_\lambda\|_{h,-1/2,\mathcal{E}_h}$ (or $\|e_\mu\|_{h,-1/2,\mathcal{E}_h}$), respectively.

We show in figure 5.6 the error curves for e_u and e_λ (left) and $\underline{e}_\sigma$ and e_μ (right) in their respective norms for the case $k = 0$. The corresponding error curves in the case $k = 1$ are shown in figure 5.7.

For the u field, the plots show second-order convergence for the interface unknowns in the case $k = 0$, while the internal unknowns are only first-order accurate. Superconvergence of the internal variables can be observed at the Gauss point. This behavior is similar to the one observed in the one-dimensional case. For the $\underline{\sigma}$ field, the plots show once again second-order convergence for the

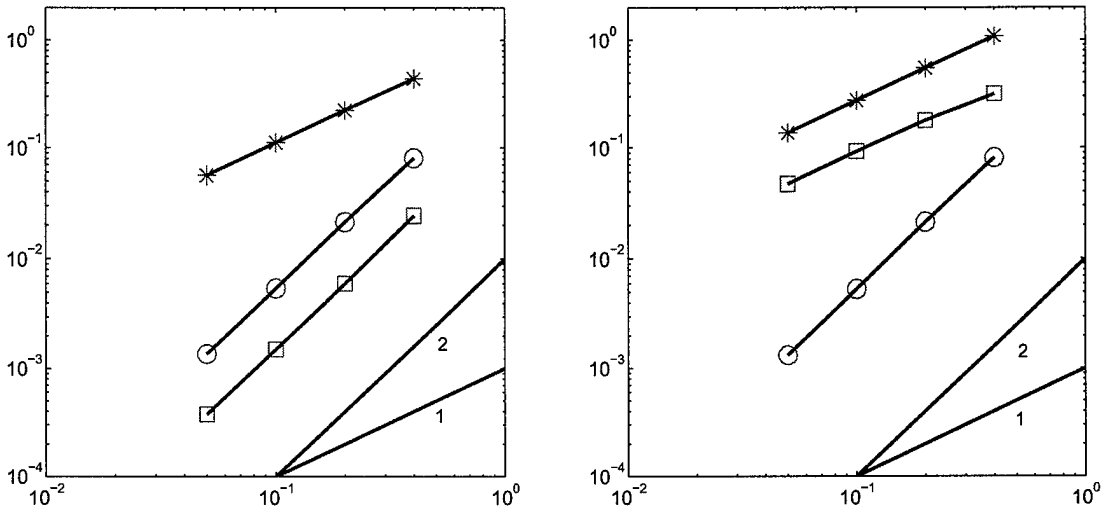

FIG. 5.6. *Two spatial dimensions. Approximation errors e_u and e_λ (left) and $\underline{e}_\sigma$ and e_μ (right) for $\mathbb{DP}_h^0$ finite elements.*

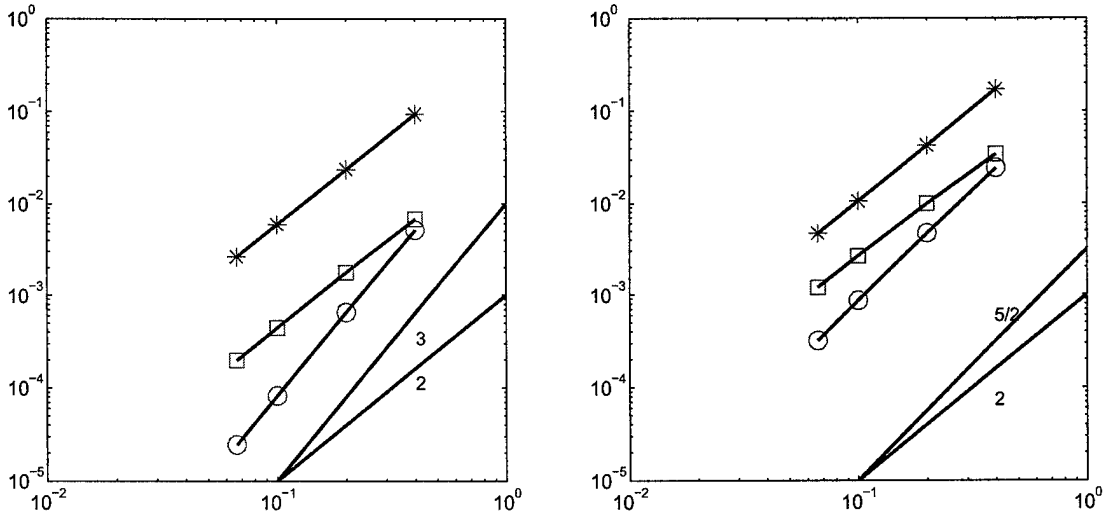

FIG. 5.7. *Two spatial dimensions. Approximation errors e_u and e_λ (left) and $\underline{e}_\sigma$ and e_μ (right) for $\mathbb{DP}_h^1$ finite elements.*

interface unknowns, while the internal unknowns are only first-order accurate. However, for this field superconvergence at the Gauss point is not observed.

In the case of $\mathbb{DP}_h^1$ finite elements, the error curves for the u field show third order accuracy for the interface unknowns, and second order accuracy for the internal unknowns. For the $\underline{\sigma}$ field, the interface unknowns achieve an order equal to approximately 5/2, while the internal variables are second-order accurate. Once again, superconvergence is not observed at the Gauss points.

In all cases, the interface unknowns are consistently more accurate than the internal fields, as expected from the one-dimensional analysis, although the exact order achieved by the various fields does not seem to obey an obvious rule. As far as the order of convergence of λ_h is concerned, the results agree with the classical convergence analysis of dual-hybrid methods. Actually in this case one obtains $\mathcal{O}(h^{k+2})$ when the Raviart-Thomas finite elements of degree k are employed (see [7], sect. V.3, formula (3.19)).

Let us conclude by comparing the performance of the DDPM approach to the performance of the standard dual method. In particular, we consider the $\mathbb{DP}_h^0$ method with static condensation versus the dual method using lowest order Raviart-Thomas finite elements ($\mathbb{D}_h^0$) with no hybridization. Table 5.1 shows the results obtained for the example here considered. The meaning of the various entries is the following: h is the value of the mesh size on the boundary of the domain, *dim* is the dimension of the matrix associated with the linear system, *nnz* is the number of non-zero elements of the same matrix and *flops* is the number of floating-point operations as computed by Matlab using sparse operations. The table on the left refers to the $\mathbb{DP}_h^0$ case, while the table on the right collects the results for the $\mathbb{D}_h^0$ case. In the first case, *flops* includes assembly, solution of the linear system and recovery of the internal fields, while in the second case it considers the sole assembly and solution phases, since there are no recoveries to perform.

TABLE 5.1
Flop counts for the $\mathbb{DP}_h^0$ and $\mathbb{D}_h^0$ methods.

h	*dim*	*nnz*	*flops*
2/5	150	662	41424
2/10	600	2713	224775
2/20	2400	11060	1835876
2/40	9600	44267	16867719

h	*dim*	*nnz*	*flops*
2/5	135	617	26888
2/10	520	2272	209964
2/20	2040	9752	2993179
2/40	8080	36112	22407438

The tables show that the $\mathbb{DP}_h^0$ method performs better than the $\mathbb{D}_h^0$ method in terms of flop-count as the dimension of the linear system grows, despite the fact that the dimension of the matrix and the number of its non-zero entries are greater than in the $\mathbb{D}_h^0$ case.

6. Conclusions. We have presented a novel mixed dual-primal finite element formulation for elliptic boundary-value problems. This work is a first attempt at generalizing discontinuous finite element formulations for generic ODE problems that were developed in previous papers. The one-dimensional formulation can be shown to lead to optimal RK methods, and therefore provides a strong incentive towards the generalization to multiple space dimensions.

The DDPM method uses interpolations of the unknown fields which are discontinuous between neighboring triangles, in the same spirit as the DG method. However, no particular expression of the numerical fluxes is selected *a priori* in this case. Additional unknowns are introduced at the element interfaces, that act as connectors gluing neighboring triangles together. The discontinuous internal unknowns can be eliminated at the element level, leaving a solution scheme in the sole interface variables. A higher rate of convergence is observed for the interface unknowns with respect to the

internal variables, as expected from the analysis in the one-dimensional case. Numerical examples have been presented to support the analysis and provide numerical evidence of the characteristics of the method here investigated.

Future efforts will concentrate on the extension of these ideas to other model problems, and on comparisons of this class of methods with alternative, well established solution procedures.

7. Acknowledgments. This research was supported by MURST Cofin '99 "Approssimazione di Problemi Non Coercivi con Applicazioni alla Meccanica dei Continui e all'Elettromagnetismo", and by the Large Scale Computing (LSC) initiative at Politecnico di Milano through the research project "IPACS: Interdisciplinary Parallel Adaptive CFD Solvers". The first author gratefully acknowledges the support and hospitality of ICASE, NASA Langley Research Center, Hampton, VA, USA.

REFERENCES

[1] D.N. ARNOLD, F. BREZZI, B. COCKBURN, AND L.D. MARINI, *Discontinuous Galerkin Methods for Elliptic Problems*, in Discontinuous Galerkin Methods, B. Cockburn, G.E. Karniadakis and C.W. Shu, eds., Lecture Notes in Computational Science and Engineering, 11, Springer, 2000, pp. 89–101.

[2] M. BORRI AND C.L. BOTTASSO, *A General Framework for Interpreting Time Finite Element Formulations*, Comp. Mech., 13 (1993), pp. 133–142.

[3] C.L. BOTTASSO, *A New Look at Finite Elements in Time: A Variational Interpretation of Runge-Kutta Methods*, Appl. Numer. Math., 25 (1997), pp. 355–368.

[4] C.L. BOTTASSO AND M. BORRI, *Some Recent Developments in the Theory of Finite Elements in Time*, Comput. Model. Simul. Engrg., 4 (1999), pp. 201–205.

[5] C.L. BOTTASSO AND A. RAGAZZI, *Finite Element and Runge-Kutta Methods for Boundary-Value and Optimal Control Problems*, J. Guid., Control & Dyn., 23 (2000).

[6] F. BREZZI, J. DOUGLAS, M. FORTIN, AND L.D. MARINI, *Efficient Rectangular Mixed Finite Elements in Two and Three Space Variables*, Math. Model. Numer. Anal., 21 (1987), pp. 581–604.

[7] F. BREZZI AND M. FORTIN, *Mixed and Hybrid Finite Element Methods*, Springer-Verlag, New York, 1991.

[8] G.F. CAREY AND J.T. ODEN, *Finite Elements: A Second Course*, Vol. II, Prentice-Hall, 1983.

[9] B. COCKBURN AND C.W. SHU, *The Local Discontinuous Galerkin Finite Element Method for Convection-Diffusion Systems*, SIAM J. Numer. Anal., 35 (1998), pp. 2440–2463.

[10] E. HAIRER, S.P. NØRSETT, AND G. WANNER, *Solving Ordinary Differential Equations I. Nonstiff Problems*, Springer-Verlag, 1987.

[11] E. HAIRER AND G. WANNER, *Solving Ordinary Differential Equations II. Stiff and Differential–Algebraic Problems*, Springer-Verlag, 1991.

[12] S. MICHELETTI AND R. SACCO, *Dual-Primal Mixed Finite Elements for Elliptic Problems*, Quaderno di Dipartimento n. 397/P, Dipartimento di Matematica "F. Brioschi", Politecnico di Milano, May 2000. To appear in Numerical Methods for Partial Differential Equations.

[13] H. RACHFORD AND M.F. WHEELER, *An H^{-1} Galerkin Procedure for the Two-Point Boundary-Value Problem*, in Mathematical Aspects of Finite Elements in Partial Differential Equations, C. De Boor, ed., Academic Press, New York, 1974, pp. 353–382.

[14] P.A. RAVIART AND J.M. THOMAS, *A Mixed Finite Element Method for Second Order Elliptic Problems*, in Mathematical Aspects of the Finite Element Method, I. Galligani, E. Magenes, eds., Lectures Notes in Math., 606, Springer-Verlag, New York, 1977, pp. 292–315.

[15] P.A. RAVIART AND J.M. THOMAS, *Primal Hybrid Finite Element Methods for 2nd Order Elliptic Equations*, Math. Comp., 31 (1977), pp. 391–413.

[16] G. SANDER AND P. BECKENS, *The Influence of the Choice of Connectors in the Finite Element Method*, in Mathematical Aspects of the Finite Element Method, I. Galligani, E. Magenes, eds., Lectures Notes in Math., 606, Springer-Verlag, New York, 1977, pp. 316–342.

[17] J.M. SANZ-SERNA AND M.P. CALVO, *Numerical Hamiltonian Problems*, Chapman & Hall, London, 1994.

[18] O.C. ZIENCKIEWICZ, *The Finite Element Method*, McGraw-Hill, London, 1977.